

Optimization of Sintering Parameters of 316L Stainless Steel for In-Situ Nitrogen Absorption and Surface Nitriding Using Response Surface Methodology

Authors:

Sadaqat Ali, Ahmad Majdi Abdul Rani, Riaz Ahmad Mufti, Syed Waqar Ahmed, Zeeshan Baig, Sri Hastuty, Muhammad Al'Hapis Abdul Razak, Abdul Azeez Abdu Aliyu

Date Submitted: 2020-05-18

Keywords: response surface methodology, nitrogen absorption, surface nitriding, sintering, 316L stainless steel

Abstract:

This research investigates the simultaneous sintering and surface nitriding of 316L stainless steel alloy using powder metallurgy method. The influence of sintering temperature and dwell time are investigated for maximum nitrogen absorption, densification and increased microhardness using response surface methodology (RSM). In this study, 316L stainless steel powder was compacted at 800 MPa and sintered at two different temperatures of 1150 and 1200 °C with varying dwell times of 1, 3, 5 and 8 h in nitrogen atmosphere. The sintered compacts were then characterized for their microstructure, densification, microhardness and nitrogen absorption. The results revealed that increased dwell time assisted nitrogen to diffuse into stainless steel matrix along with the creation of nitride layer onto the sample surface. The microhardness and density also increased with increasing dwell time. A densification of 7.575 g/cm³ and microhardness of 235 HV were obtained for the samples sintered at 1200 °C temperature with 8 h dwell time. The simultaneous sintering and surface nitriding technique developed in this research work can help in improving corrosion resistance of this material and controlling leaching of metal ions for its potential use in biomedical applications.

Record Type: Published Article

Submitted To: LAPSE (Living Archive for Process Systems Engineering)

Citation (overall record, always the latest version):

LAPSE:2020.0441

Citation (this specific file, latest version):

LAPSE:2020.0441-1

Citation (this specific file, this version):

LAPSE:2020.0441-1v1

DOI of Published Version: <https://doi.org/10.3390/pr8030297>

License: Creative Commons Attribution 4.0 International (CC BY 4.0)

Article

Optimization of Sintering Parameters of 316L Stainless Steel for In-Situ Nitrogen Absorption and Surface Nitriding Using Response Surface Methodology

Sadaqat Ali ^{1,*} , Ahmad Majdi Abdul Rani ^{2,*}, Riaz Ahmad Mufti ¹, Syed Waqar Ahmed ³, Zeeshan Baig ⁴, Sri Hastuty ⁵, Muhammad Al'Hapis Abdul Razak ⁶ , and Abdul Azeez Abdu Aliyu ⁷

¹ School of Mechanical & Manufacturing Engineering, National University of Sciences and Technology (NUST), H-12, Islamabad 44000, Pakistan; riazmufti@smme.nust.edu.pk

² Mechanical Engineering Department, Universiti Teknologi PETRONAS (UTP), Seri Iskandar 32610, Malaysia

³ Department of Mechanical Engineering, Ghulam Ishaq Khan Institute of Engineering Sciences and Technology, Khyber Pakhtunkhwa 19201, Pakistan; waqarg05@gmail.com

⁴ Centre of Excellence in Science & Applied Technologies, Islamabad 44000, Pakistan; meteng81@gmail.com

⁵ Mechanical Engineering Department, Universitas PERTAMINA, Jakarta 12220, Indonesia; sri.hastuty@universitaspertamina.ac.id

⁶ Manufacturing Section, Universiti Kuala Lumpur Malaysian Spanish Institute, Kulim Hi-Tech Park, Kedah 09000, Malaysia; alhapis@unikl.edu.my

⁷ Mechanical Engineering Department, Bayero University Kano, Kano 700241, Nigeria; garoabdul@gmail.com

* Correspondence: engineersadaqat@gmail.com (S.A.); majdi@utp.edu.my (A.M.A.R.)

Received: 11 January 2020; Accepted: 25 February 2020; Published: 5 March 2020



Abstract: This research investigates the simultaneous sintering and surface nitriding of 316L stainless steel alloy using powder metallurgy method. The influence of sintering temperature and dwell time are investigated for maximum nitrogen absorption, densification and increased microhardness using response surface methodology (RSM). In this study, 316L stainless steel powder was compacted at 800 MPa and sintered at two different temperatures of 1150 and 1200 °C with varying dwell times of 1, 3, 5 and 8 h in nitrogen atmosphere. The sintered compacts were then characterized for their microstructure, densification, microhardness and nitrogen absorption. The results revealed that increased dwell time assisted nitrogen to diffuse into stainless steel matrix along with the creation of nitride layer onto the sample surface. The microhardness and density also increased with increasing dwell time. A densification of 7.575 g/cm³ and microhardness of 235 HV were obtained for the samples sintered at 1200 °C temperature with 8 h dwell time. The simultaneous sintering and surface nitriding technique developed in this research work can help in improving corrosion resistance of this material and controlling leaching of metal ions for its potential use in biomedical applications.

Keywords: 316L stainless steel; sintering; surface nitriding; nitrogen absorption; response surface methodology

1. Introduction

Among the commonly used biomaterials, 316L stainless steel is in use since ancient times when total hip replacement of a patient was carried out using 316L stainless steel for implantation [1,2]. Since then, 316L stainless steel has been gaining great attention in biomedical applications. It is available at a low cost with adequate mechanical properties, biocompatibility and corrosion resistance [3,4].

The implants and medical devices can be manufactured from 316L stainless steel at a relatively low cost as compared to its counterpart materials including cobalt chromium, titanium and other biomaterials [5–10]. Austenitic 316L stainless steel is also recommended by ASTM International for use in implant manufacturing and medical devices [11–13]. The low carbon content and high chromium concentration in this material makes it resistant to corrosive environment specially in chlorine bearing solutions [14]. The human body saline resembles the chlorine bearing solution making this material an ideal choice for usage in implant manufacturing [15].

The 316L stainless steel contains 10%–14% nickel for promoting the austenitic structure [16]. It has been reported that the implants made of biomaterials have been reported to be associated with release of metal ions and debris due to poor surface finish and corrosion resistance [17,18]. Among the released metal ions, nickel and chromium have been proven to be the cause of many genotoxic and mutagenic activities [19]. Nickel has been associated with contact allergy for patients allergic to metals causing skin diseases including dermatitis and eczematous rash [16,19]. The leaching of ions and debris due to ionic leaching have been reported to be the cause of swelling and localized pain due to inflammation [20]. The leaching of metal ions demands the surface improvement of 316L stainless steel implant material [21,22]. Various methods have been developed to improve the surface quality and corrosion resistance of stainless-steel including surface modification techniques. These include physical, chemical and mechanical surface modification techniques [23,24]. However, certain disadvantages are associated with these techniques which limit their application in biomedical field including low coating deposition rate, crack free coatings, line of sight and expensive raw materials [25,26]. To overcome these shortcomings and develop an alternative solution, optimization of sintering parameters for surface nitriding of the material can address these issues [27–29]. The optimal sintering parameters with increased dwell time can help in creating a protective surface layer on the stainless-steel surface. This will help in improving the corrosion resistance of the material and act as an inhibitor for controlling the leaching of ions.

2. Materials and Methods

In this research, commercially available pure irregular shape water atomized 316L stainless steel powder was selected due to high packing density and better sinter ability than gas atomized powder. The chemical composition of the powder has been summarized in Table 1. The particle size distribution of the powder was characterized and is presented in Table 2.

Table 1. Chemical composition of 316L stainless steel powder used in the study.

Element	C	Si	O	Mn	Ni	Cr	Mo	Fe
wt.%	0.028	0.9	0.068	1.5	12.01	17.04	2.4	Balance

Table 2. Particle size distribution of 316L stainless steel powder.

Particle Distribution	D10	D50	D90
Particle size (μm)	3.98	10.27	19.61

Uniaxial cold compaction process was used to prepare the samples of size 30 mm diameter and 5 mm thickness using stainless steel die. The powder was compressed at 800 MPa pressure to prepare the green compacts followed by sintering in nitrogen atmosphere at two different temperatures of 1150 and 1200 °C. The dwell time was varied for each temperature and was set at 1, 3, 5 and 8 h. The SEM and XRD of the powder have been presented in Figures 1 and 2 respectively.

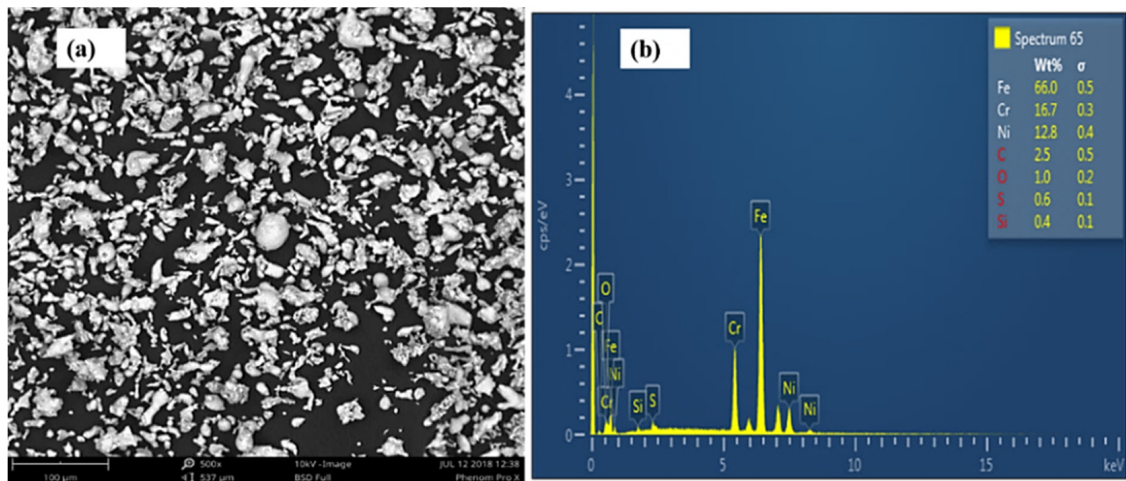


Figure 1. SEM (a) and EDX (b) of 316L stainless steel powder.

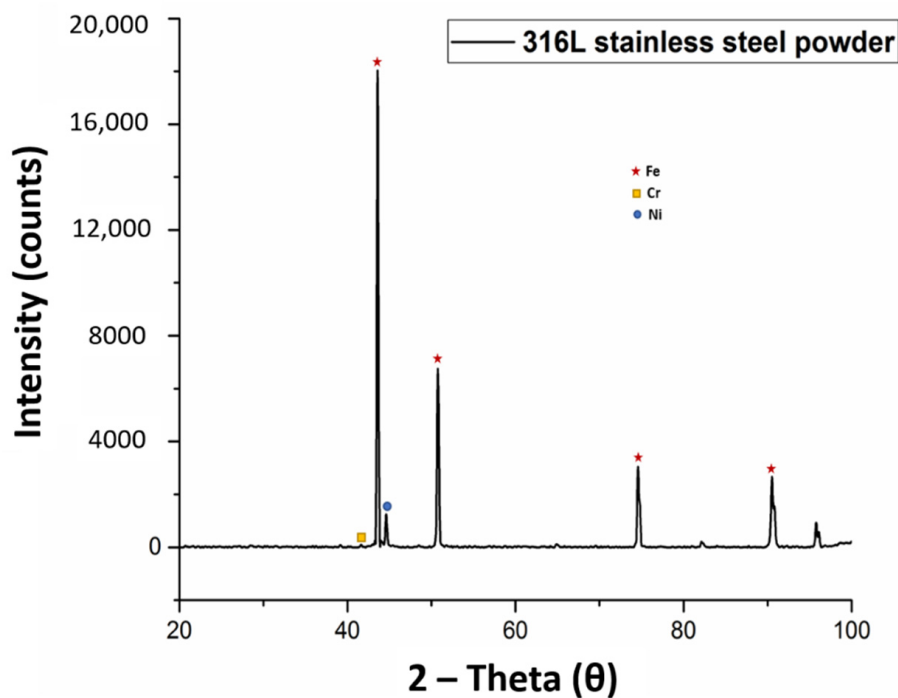


Figure 2. XRD spectrum of 316L stainless steel powder.

The most influential parameter settings, optimizing and generating a mathematical model for the selected responses was carried out by response surface methodology (RSM) (D-optimum custom design). This design generates a design that estimates the influence of the process parameters in the best possible way, particularly suited for screening studies. Considering the role of nitrogen absorption (N-abs), density (D) and microhardness (HV) in developing suitable implant material and the capability of powder metallurgy process, three major responses (N-abs, D and HV) were selected for parameters optimizations. The two important factors influencing these responses namely sintering temperature (St) and dwell time (Dt) and mixed level design were used to plan the experiment. A total of 16 experimental runs were conducted according to the procedure described above and have been presented in Table 3.

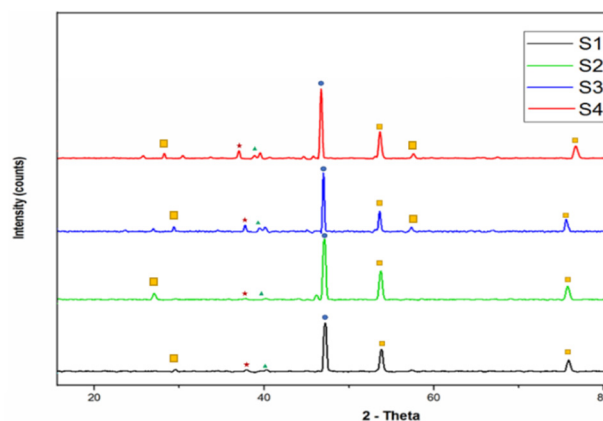
Table 3. Design of Experiments (DOE) matrix and experimental results for the responses.

Run Order	Sintering Temperature (°C)	Dwell Time (hours)	Nitrogen Absorption (%)	% of Theoretical Density	Sintered Density (g/cm ³)	Micro Hardness (HV)
1	1150	5	1.61	92.74	7.410	203
2	1200	1	1.04	92.01	7.352	185
3	1156	8	2.41	93.82	7.497	229
4	1150	5	1.61	92.74	7.410	203
5	1178	8	2.56	94.11	7.520	231
6	1158	3	1.10	92.20	7.367	196
7	1200	5	1.93	94.80	7.575	210
8	1175	3	1.20	92.30	7.375	197
9	1175	3	1.20	92.30	7.375	197
10	1178	8	2.56	94.11	7.520	231
11	1200	5	1.61	94.80	7.575	231
12	1167	1	0.98	91.73	7.330	182
13	1192	3	1.26	92.35	7.379	198
14	1175	3	1.20	92.30	7.375	197
15	1200	8	2.82	94.80	7.575	235
16	1150	1	0.96	91.58	7.318	180

The sintered samples were then characterized using X-ray diffractometer (Model: X'pert3, Powder and Empyrean, PANalytical, B.V, Lelyweg, Almelo, The Netherlands), X-ray photoelectron spectrometer (Model: Thermo Scientific, K-alpha, East Grinstead, UK), optical microscope (Model: Leica DM LM, Wetzlar, Germany) and Vickers hardness tests using tester (Model: Leco LM 247AT, St Joseph, MI, USA) to examine the resulting properties of the sintered samples.

3. Results and Discussion

The XRD evaluation was carried out to analyze the diffusion of nitrogen into the matrix of the sintered samples. The results indicated that the sintering atmosphere and dwell times helped in diffusing nitrogen to form strong nitrides with the constituents of 316L stainless steel matrix. The XRD spectrum of the sintered samples have been presented in Figure 3, indicating S1 sample sintered for 1 h dwell time, S2 sintered for 3 h dwell time, S3 sintered for 5 h dwell time and S4 sintered at dwell time of 8 h at sintering temperature of 1200 °C. The results indicate the formation of C₃N₄ at d spacing of 2.51960 Å, FeN_{0.324} at d spacing of 2.07500 Å, Cr₂O₃ at d spacing of 2.66348 Å and Ni (Cr₂O₄) at d spacing of 2.49354 Å. The presence of γFe in all the samples indicated that the austenitic structure of the 316L stainless steel was retained at increased dwell times.

**Figure 3.** XRD spectra of sintered samples at different dwell times.

The XPS was done to analyze the existence of nitrogen onto the sample surface. The results indicated that the dwell time has a notable effect on the amount of nitrogen on surface of the sample. The amount of nitrogen increased with increasing dwell time and a maximum of 2.82% nitrogen was observed for samples sintered at 1200 °C temperature and 8 h dwell time. The XPS analysis has been presented in Figure 4.

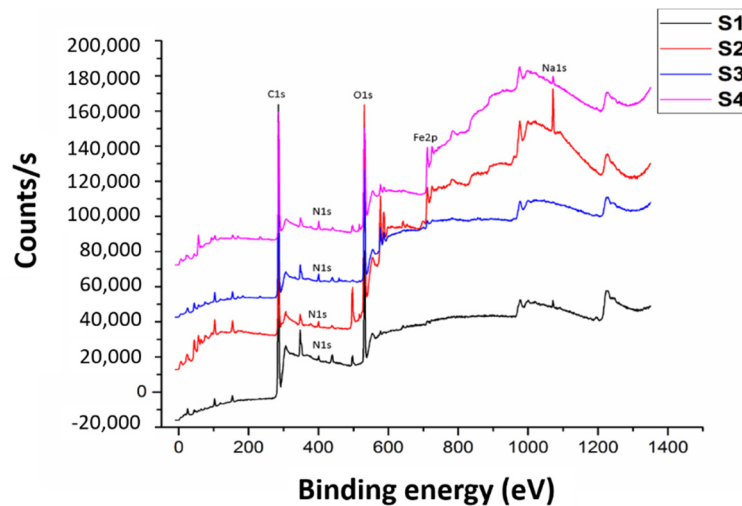


Figure 4. XPS analysis of sintered samples at different dwell times.

The microstructure of the sintered samples was observed under optical microscope after complete metallographic preparation. The micrographs of the sintered samples as viewed from optical microscope have been presented in Figure 5, indicating S1 sample sintered for 1 h dwell time, S2 sintered for 3 h dwell time, S3 sintered for 5 h dwell time and S4 sintered at dwell time of 8 h at sintering temperature of 1200 °C. It can be observed from the micrographs that the samples are sintered properly with clear grain boundaries. Moreover, increased sintering dwell time helped in creation of clear grain boundaries with reduced porosity as observed in the micrographs.

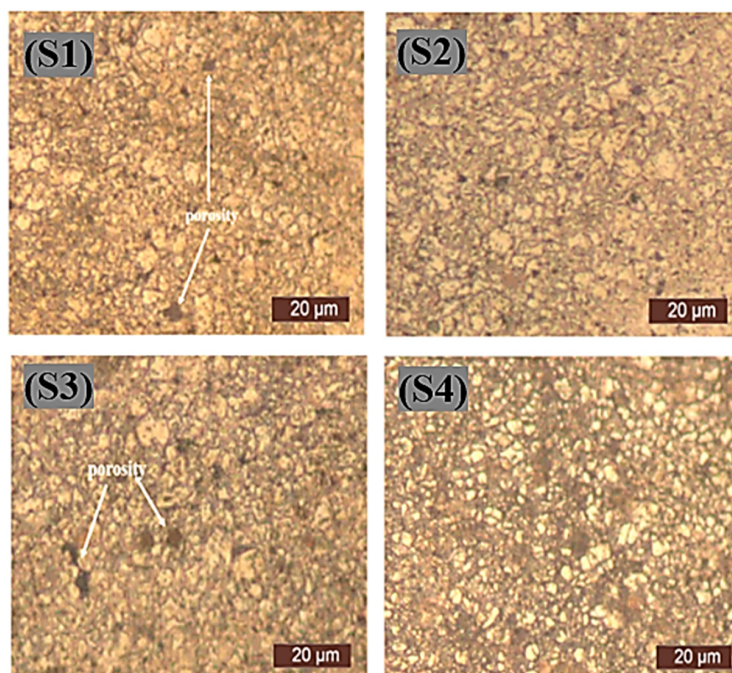


Figure 5. Microstructure of the sintered samples.

The FESEM (Field Emission Scanning Electron Microscope) of sintered samples was done to further explore the effect of sintering parameters and presence of nitrogen. The elemental mapping was held for different elements present in the stainless steel. It was also helpful in identifying the effect of prolonged sintering dwell time. The results indicated the occurrence of nitrogen in the samples indicating that nitrogen diffused into the stainless steel matrix. The elemental mapping of the selected sample has been demonstrated in the Figure 6.

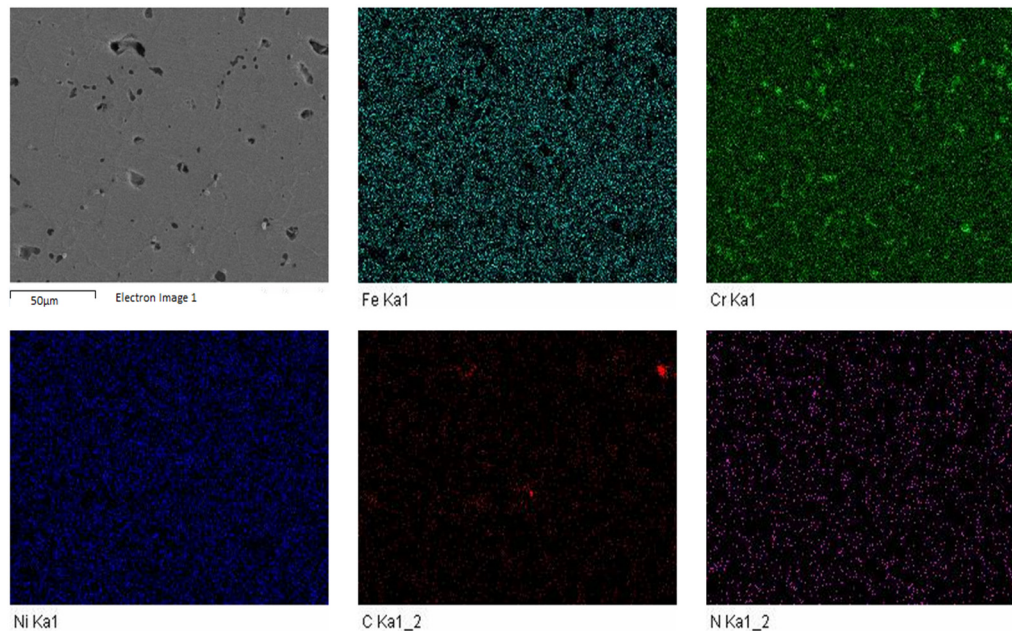


Figure 6. FESEM-EDS elemental maps for sample sintered at 8 h dwell time.

The increased dwell time of sintering created a strong nitride layer onto the surface of the sample. The parameters of sintering simultaneously sintered and surface nitride the samples. The nitride layer developed onto the sample surface improves the corrosion resistance of the material along with controlling the leaching of metal ions during exposure to corrosive environments. The nitride layer formation of selected sample has been illustrated in Figure 7.

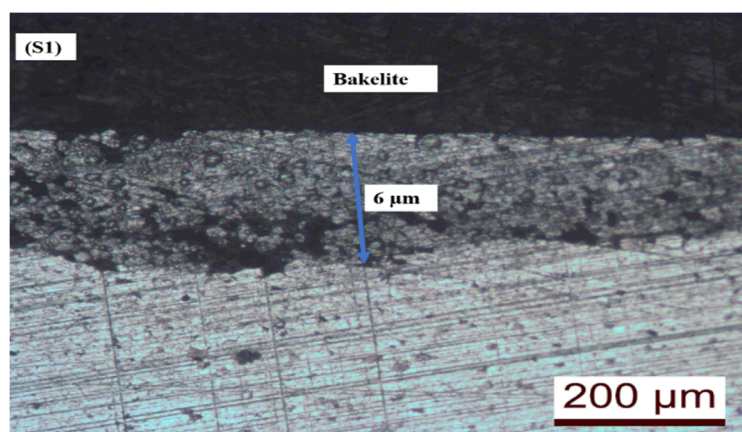


Figure 7. Surface nitride layer of sintered samples.

The microhardness of the sintered samples was measured using Vickers hardness testing whereby, 200 gf was applied on the polished surface sample for a time period of 15 s. The microhardness value of 185 HV was measured for 1 h dwell time sintered sample, whereas its value increased to 235 HV for 8 h dwell time sintered samples. The increased absorption of nitrogen at increased dwell times can be

attributed to the increase of microhardness values. The microhardness values of the sintered samples have been presented in Figure 8.

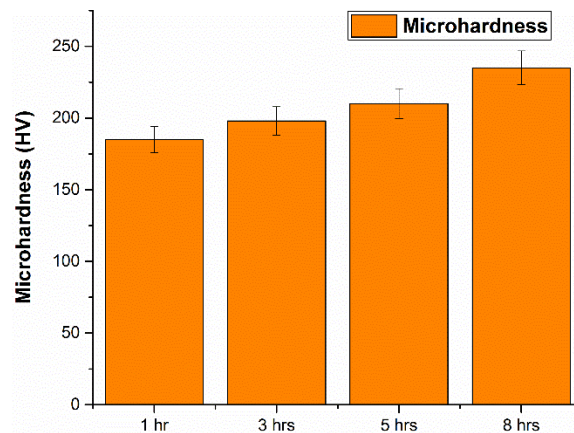


Figure 8. Microhardness values of sintered samples at varying dwell times.

3.1. Influence of Input Parameters on Nitrogen Absorption

The impact of process parameters on nitrogen absorption was determined using D-optimum design analysis. The analysis of variance (ANOVA) for the nitrogen absorption has been presented in Table 4. The regression model, significant factors, interactions and lack of fit are summarized. The model and the model terms with the values of “prob > F” less than 0.0500 are considered as significant terms. It can be noticed from the ANOVA table that the factors St and Dt are significant model terms for nitrogen absorption. The lack of fit “prob > F” value of 0.7039 employs that it is non-significant. The difference between adjusted R-square predicted R-square shows that the terms are in reasonable agreement with each other as presented in Table 5.

Table 4. ANOVA for nitrogen absorption.

Source	Sum of Squares	df	Mean Square	F Value	p-Value Prob > F	Significance
Model	2.03	5	0.41	154.42	<0.0001	significant
A-St	0.024	1	0.024	9.25	0.0125	
B-Dt	1.82	1	1.82	689.78	<0.0001	
AB	6.5×10^{-4}	1	6.5×10^{-4}	0.25	0.6298	
A ²	9.91×10^{-3}	1	9.91×10^{-3}	3.77	0.0810	
B ²	9.93×10^{-3}	1	9.93×10^{-3}	3.77	0.0808	
Residual	0.026	10	2.63×10^{-3}			
Lack of fit	9.9×10^{-3}	5	1.98×10^{-3}	0.60	0.7039	not significant
Pure Error	0.016	5	3.28×10^{-3}			
Cor Total	2.06	15				

Table 5. Predicted R-square vs. adjusted R-square.

Std. Dev.	0.051	R-squared	0.9872
Mean	0.42	Adj R-squared	0.9808
C.V.%	12.19	Pred R-squared	0.9731
PRESS	0.055	Adeq Precision	35.175
−2 Log Likelihood	−57.14		

Most of the data was found to lie along straight line as observed in the normal probability plot of residuals shown in Figure 9a. This indicated the selected model terms are only significant factors and the errors are normally distributed.

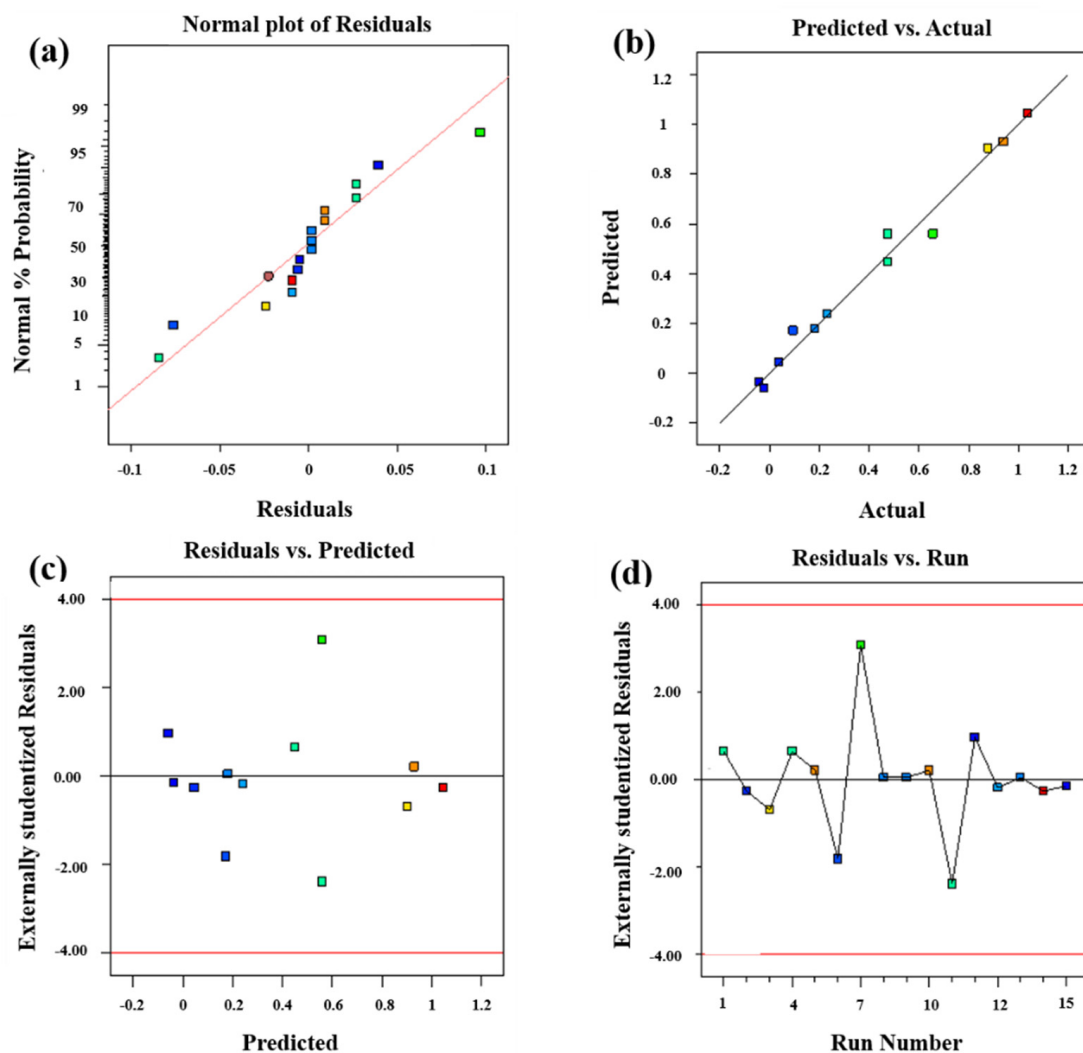


Figure 9. (a) Normal plot of residuals (b) predicted vs. actual plot (c) residuals vs. predicted plot (d) residuals vs. run plot.

A well fitted regression which scattered along straight line could be observed in the predicted (software calculated) versus actual (experimental) values plot shown in Figure 9b. This confirmed that the model is very well designed. A non-clear pattern and randomly scattered data as required was observed in the residual versus predicted values plot (Figure 9c). To measure the number of the standard deviation, an internally studentized residuals is calculated by taking the ratio between the residuals to that of the residuals of estimated standard deviation. The residual values are obtained by calculating the difference between measured and predicted values. The plot of residuals versus internally studentized residuals presented in Figure 9d confirmed that all values lie within limits and that the model can be used to predict the response.

The one factor effect plot for nitrogen absorption has been depicted in Figure 10. The one factor plot helps in predicting the behavior of each output by changing the respective input parameter. It can be noticed that increase in the dwell time from 1 h to 8 h results in increased nitrogen absorption values as shown in Figure 10d–f. The increase in sintering temperature also resulted in increased nitrogen absorption and can be observed in Figure 10a–c.

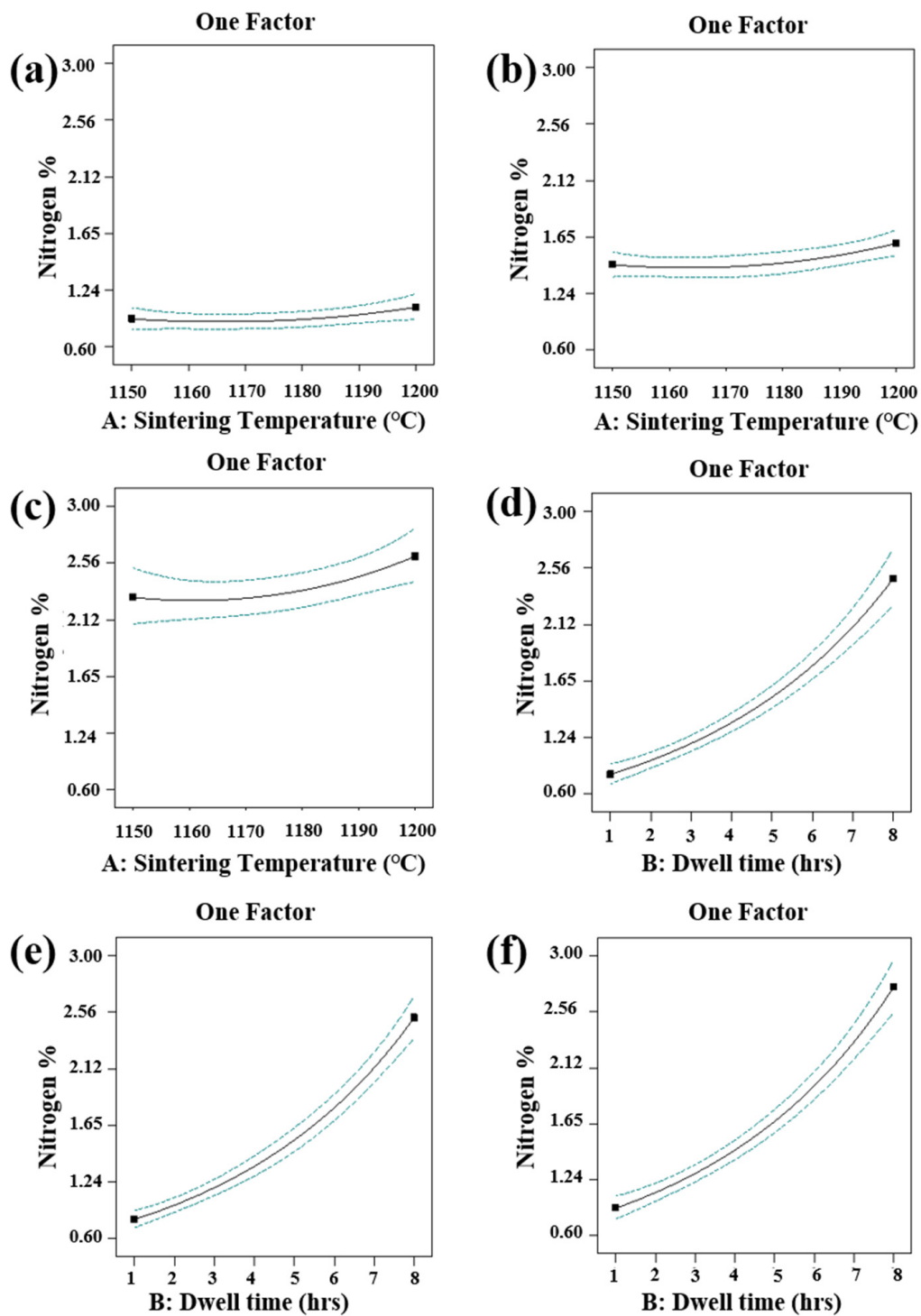


Figure 10. One factor effect plot for nitrogen absorption.

The two-dimensional representation of nitrogen absorption for the selected parameters is shown by the contour plot presented in Figure 11a. The nitrogen absorption values indicated in the middle of each contour increases linearly from the first to the last contour. The influence of sintering parameters on nitrogen absorption in the form of a three-dimensional (3D) surface plot has been presented in Figure 11b. The plot shows that nitrogen absorption increases with increase of sintering temperature and dwell time.

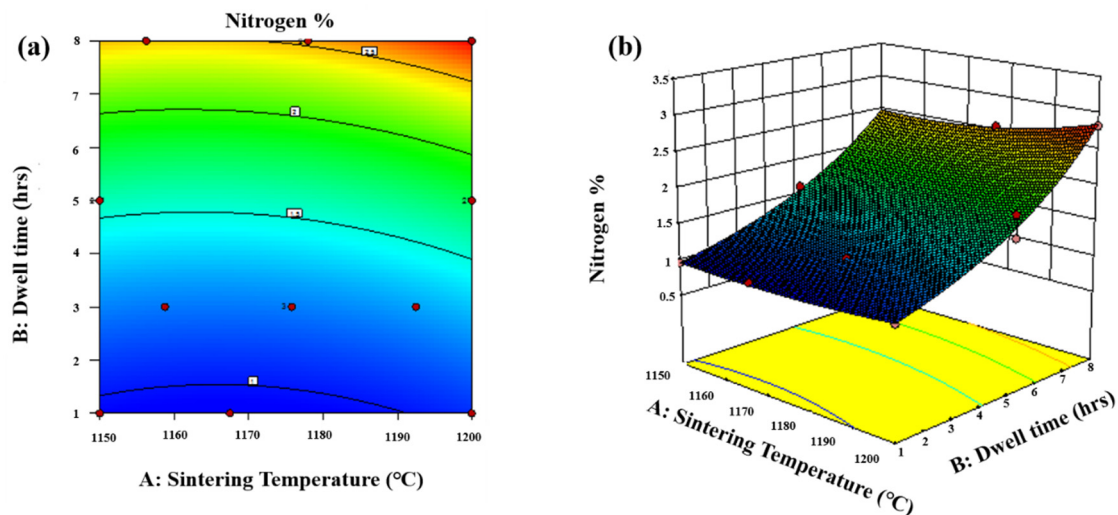


Figure 11. Contour and three-dimensional (3D) plots of nitrogen absorption.

3.2. Influence of Input Parameters on Density

The ANOVA table indicating the contribution of each factor on density is presented in Table 6. It signifies the significance of the model since “Prob > F” value is 0.0001. The table also shows that the factors St and Dt are significant model terms with “Prob > F” values <0.05.

Table 6. ANOVA for density.

Source	Sum of Squares	df	Mean Square	F Value	<i>p</i> -Value Prob > F	Significance
Model	2.132×10^{-3}	5	4.264×10^{-4}	23.66	<0.0001	significant
A-St	3.695×10^{-4}	1	3.695×10^{-4}	20.50	0.0011	
B-Dt	1.457×10^{-3}	1	1.457×10^{-3}	80.83	<0.0001	
AB	3.56×10^{-5}	1	3.568×10^{-5}	1.98	0.1897	
A2	6.941×10^{-5}	1	6.941×10^{-5}	3.85	0.0781	
B2	2.847×10^{-5}	1	2.847×10^{-5}	1.58	0.2374	
Residual	1.802×10^{-4}	10	1.802×10^{-5}			
Lack of fit	1.802×10^{-4}	5	3.604×10^{-5}			
Pure Error	0.000	5	0.000			
Cor Total	2.312×10^{-3}	15				

The value of 0.7315 for predicted R-square indicates that it lies within acceptable range to that of adjusted R-square as shown in Table 7. The value “Adeq precision” of 16.423 is good for a suitable signal indicating that the model can be employed to navigate the design space.

Table 7. Predicted R-square vs. adjusted R-square.

Std. Dev.	4.24×10^{-3}	R-squared	0.9221
Mean	2.01	Adj R-squared	0.8831
C.V.%	0.21	Pred R-squared	0.7315
PRESS	6.209×10^{-4}	Adeq Precision	16.423
−2 Log Likelihood	−136.90		

The normal probability plot of the residuals plot shows that nearly all the data lies along a straight line as shown in Figure 12a. A well fitted regression which scattered along straight line could be observed in the predicted (software calculated) versus actual (experimental) values plot shown in Figure 12b. This confirmed that the selected terms are only significant factors and the errors are

normally distributed. The residuals versus predicted values plot shows a randomly distributed data as shown in Figure 12c. The studentized residuals of regression lines of residuals versus run plot lie within the limits as shown in Figure 12d. This confirms the capability of the model to predict the density.

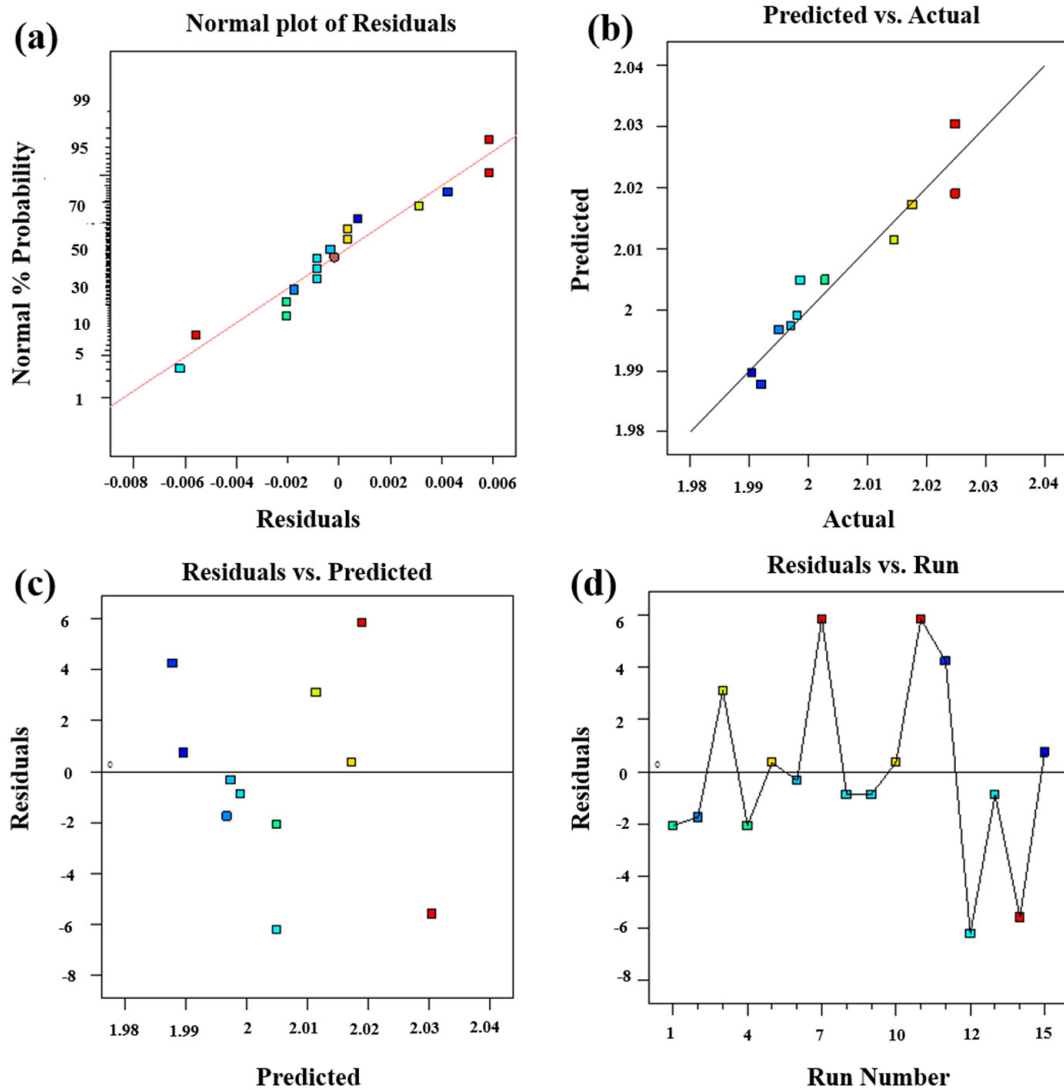


Figure 12. (a) Normal plot of residuals (b) predicted vs. actual plot (c) residuals vs. predicted plot (d) residuals vs. run plot.

The one factor effect plot for density has been presented in Figure 13. It can be observed that increased dwell time from 1 h to 8 h results in increased density value as shown in Figure 13d–f. The increase in sintering temperature also has also a notable effect on the densification as can be seen in Figure 13a–c.

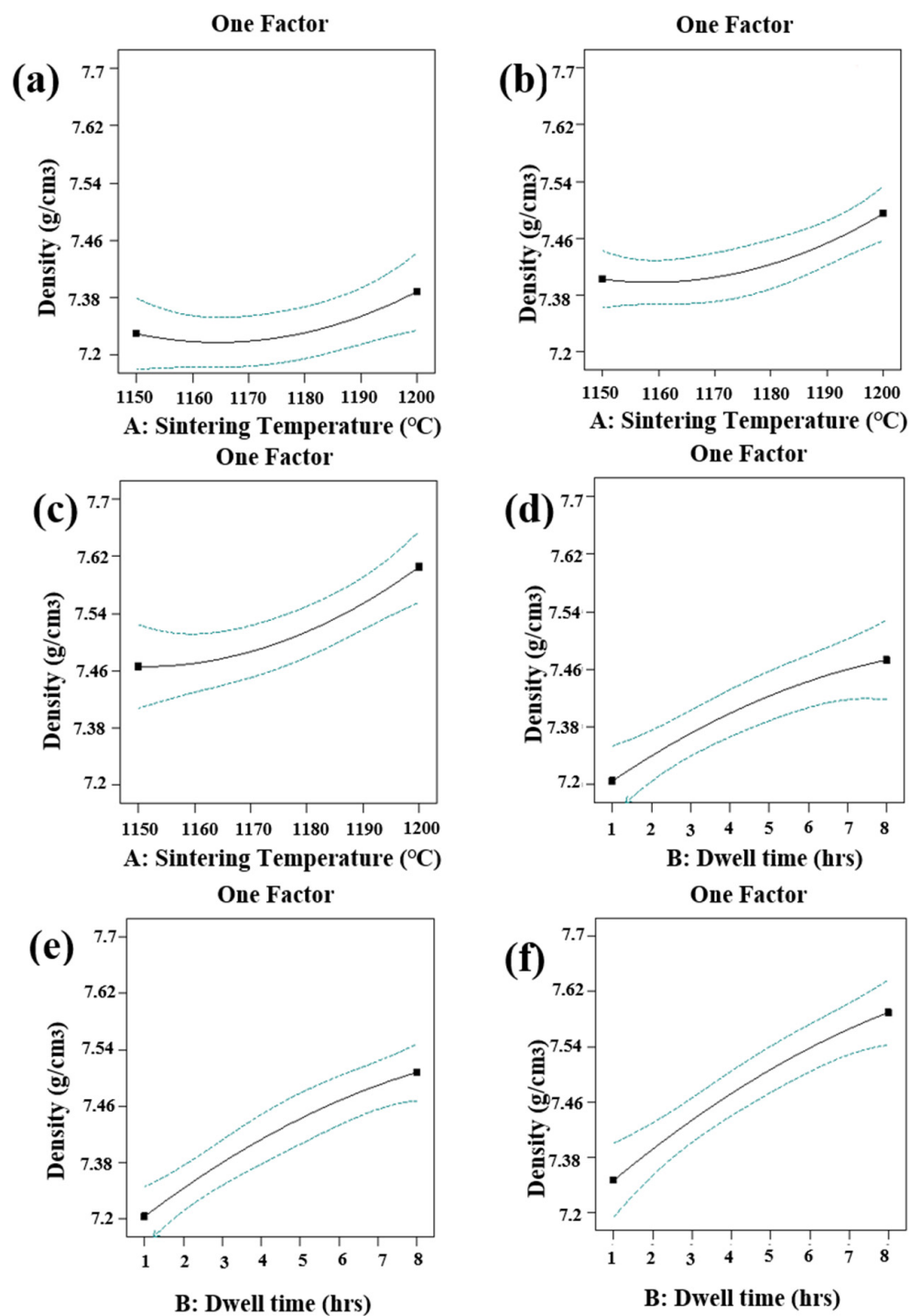


Figure 13. One factor effect plot for density.

The two-dimensional representation of density for the selected parameters is shown by the contour plot presented in Figure 14a. The influence of sintering parameters on densification in the form of 3D surface plot has been presented in Figure 14b. The plot shows that density increases with increase of sintering temperature and dwell time.

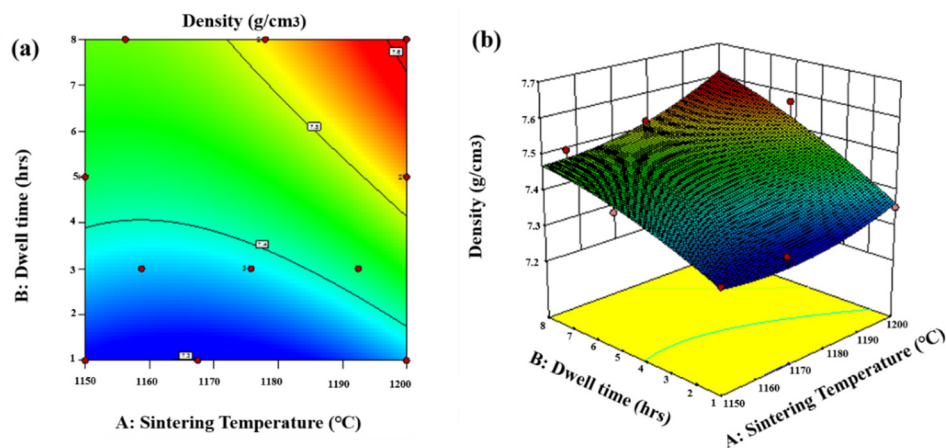


Figure 14. Contour and 3D plots of density.

3.3. Influence of Input Parameters on Microhardness

The impact of process parameters on microhardness was determined using D-optimum design analysis. The analysis of variance (ANOVA) for microhardness has been presented in Table 8. The model and the model terms with the values of “prob > F” less than 0.0500 are considered as significant terms. It can be noticed from the ANOVA table that the factors St and Dt are significant model terms for microhardness. The model is expected to fit, the reason being the lack of fit “prob > F” value of 0.9126 employs that it is non-significant. The difference between adjusted R-square and predicted R-square shows that the terms are in reasonable agreement with each other as seen in Table 9.

Table 8. ANOVA for microhardness.

Source	Sum of Squares	df	Mean Square	F Value	p-Value Prob > F	Significance
Model	0.12	3	0.039	71.38	<0.0001	significant
A-St	5.825×10^{-3}	1	5.825×10^{-3}	10.58	0.0069	
B-Dt	0.11	1	0.11	192.71	<0.0001	
AB	9.377×10^{-5}	1	9.377×10^{-5}	0.17	0.6871	
A2	6.607×10^{-3}	12	5.506×10^{-4}			
B2	2.065×10^{-3}	7	2.950×10^{-4}	0.31	0.9126	not significant
Residual	4.542×10^{-3}	5	9.084×10^{-4}			
Lack of fit	0.12	15	0.039			
Pure Error	0.12	3	5.825×10^{-3}			
Cor Total	5.825×10^{-3}	1				

Table 9. Predicted R-square vs. adjusted R-square.

Std. Dev.	0.023	R-squared	0.9469
Mean	5.33	Adj R-squared	0.9337
C.V.%	0.44	Pred R-squared	0.9055
PRESS	0.012	Adeq Precision	24.226
−2 Log Likelihood	−79.27		

Most of the data was found to lie along straight line as observed in the plot of residuals for normal probability and can be seen in Figure 15a. This indicated the selected model terms are only significant factors and the errors are normally distributed.

A well fitted regression which scattered along straight line could be observed in the predicted (software calculated) versus actual (experimental) values plot shown in Figure 15b. This confirmed that the model is very well designated. A non-clear pattern and randomly scattered data as required

was observed in the residual versus predicted values plot (Figure 15c). To measure the number of the standard deviations between predicted and actual values, an internally studentized residuals is calculated by taking the ratio between the residuals to that of the residuals of estimated standard deviation. The residual values are obtained by calculating the difference between measured and predicted values. The plot of residuals versus internally studentized residuals shown in Figure 15d verified that the model can be used to predict the response, due to the absence of any outlier and all the values lie within the limits.

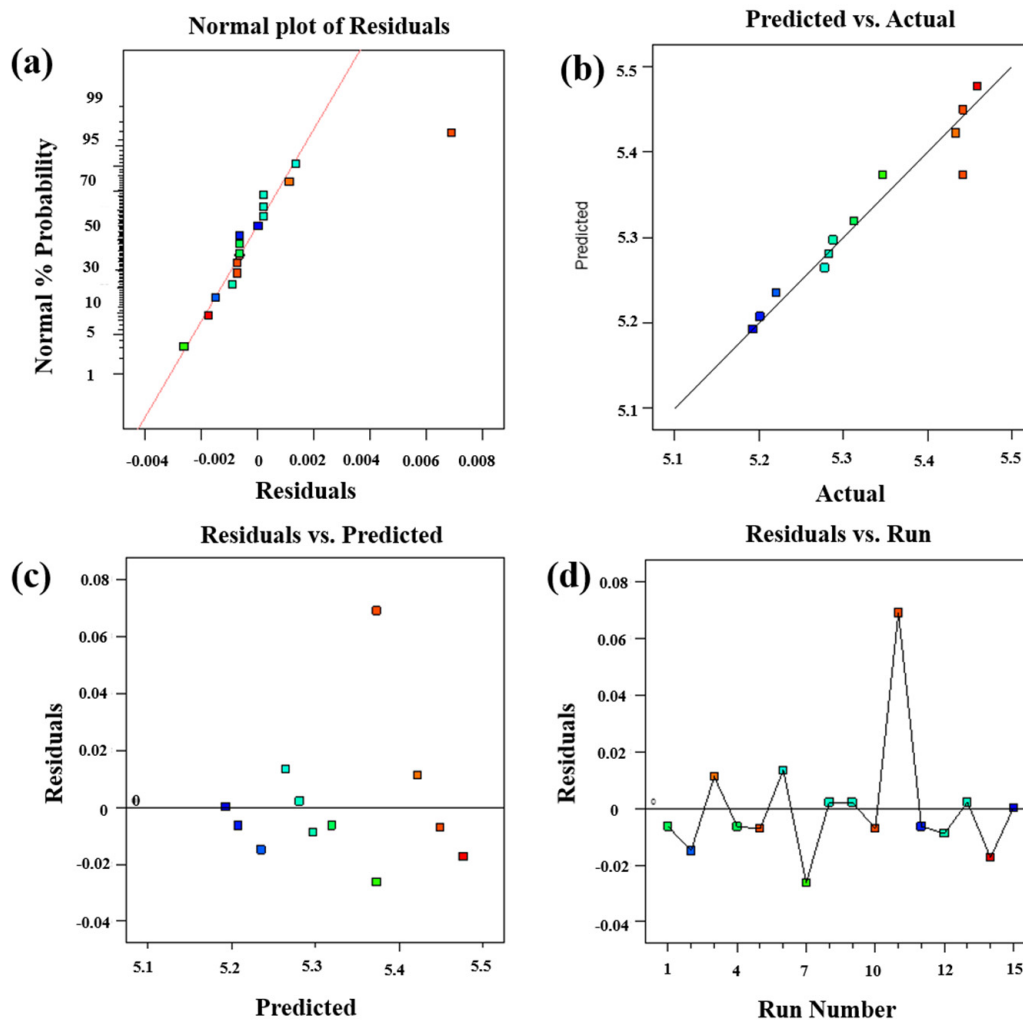


Figure 15. (a) Normal plot of residuals (b) predicted vs. actual plot (c) residuals vs. predicted plot (d) residuals vs. run plot.

The one factor effect plot for micro hardness has been depicted in Figure 16. It can be noticed that increase in the dwell time from 1 h to 8 h results in increased micro hardness values as shown in Figure 16d–f. The increase in sintering temperature also has a notable effect on the increased nitrogen absorption as can be seen in Figure 16a–c.

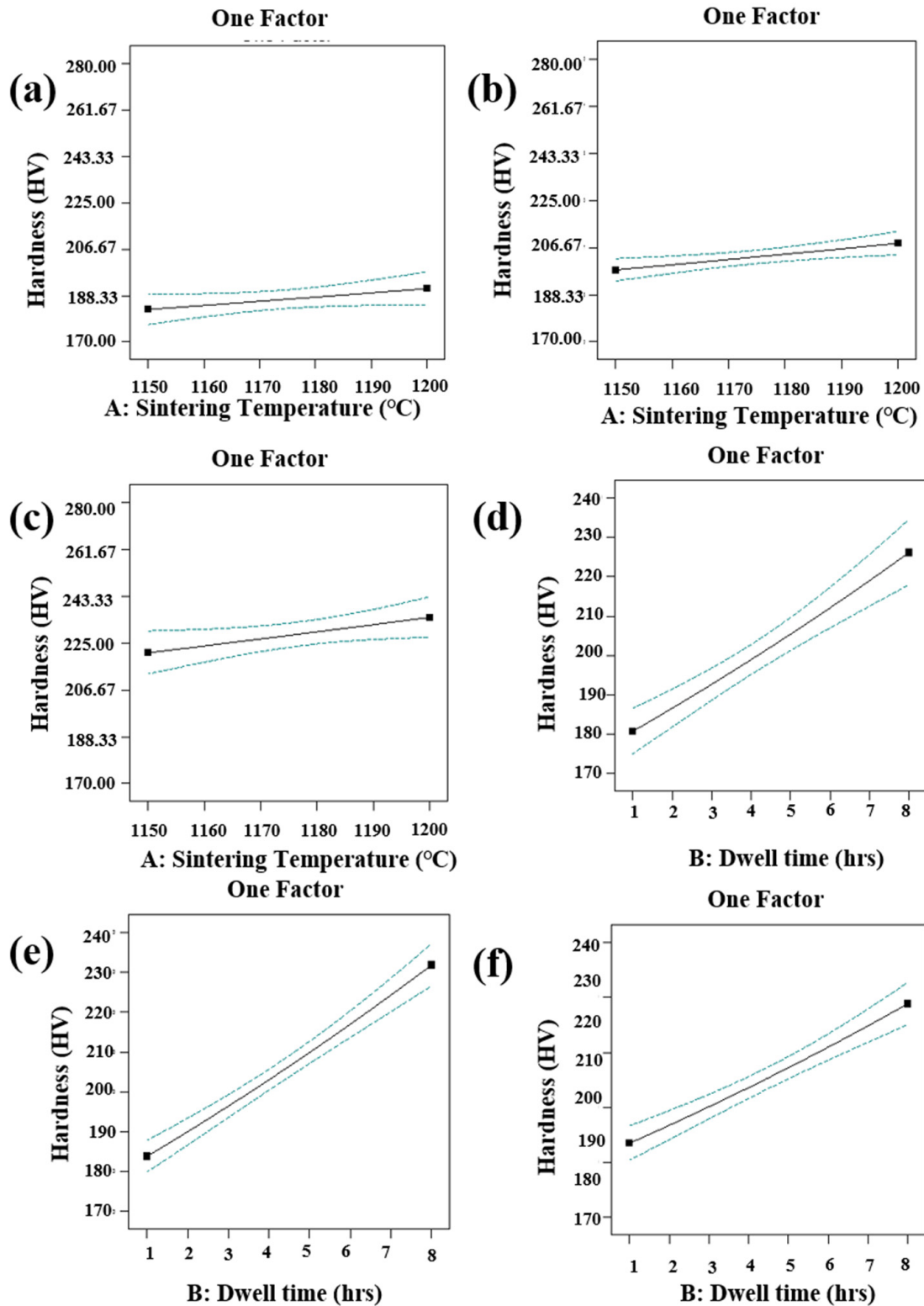


Figure 16. One factor effect plot for micro hardness.

The two-dimensional representation of micro hardness for the selected parameters is shown by the contour plot presented in Figure 17a. The nitrogen absorption values indicated in the middle of each contour increases linearly from the first to the last contour. The influence of sintering parameters on microhardness in the form of 3D surface plot has been presented in Figure 17b. The plot shows that nitrogen absorption increases with increase of sintering temperature and dwell time.

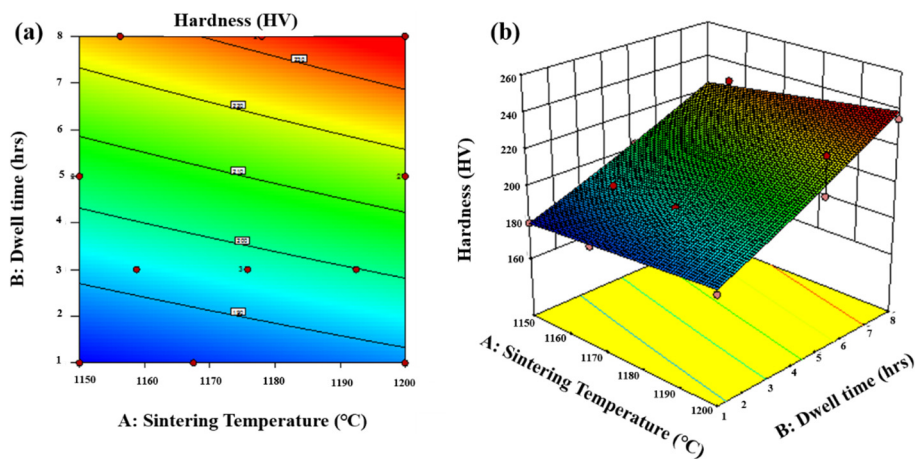


Figure 17. Contour and 3D plots of microhardness.

4. Modelling of Responses

The ANOVA tables discussed in the previous sections developed the equations which relate the responses nitrogen absorption (N-abs), density (D) and micro hardness (HV) and the input parameters. The final predicted model equations in terms of the actual factors for N-abs, D and HV are presented in the equations below.

4.1. Predicted Model Equation for Nitrogen Absorption

The predicted model equation for nitrogen absorption from the analysis has been presented in the Equation (1).

$$\begin{aligned} \ln(\text{N-abs}) = & +124.27050 - 0.21326 * \text{St} - 0.078854 * \text{Dwell time} + 1.49490 \times 10^{-4} \\ & * \text{St} * \text{Dt} + 9.1380 \times 10^{-5} * \text{St}^2 + 4.71247 \times 10^{-3} * \text{Dt}^2 \end{aligned} \quad (1)$$

4.2. Predicted Model Equation for Density

The predicted model equation for density from the analysis has been presented in Equation (2).

$$\begin{aligned} \ln(D) = & +12.40992 - 0.017856 * \text{St} - 0.034901 * \text{Dwell time} + 3.49901 \times 10^{-5} \\ & * \text{St} * \text{Dt} + 7.64426 \times 10^{-6} * \text{St}^2 - 2.52253 \times 10^{-4} * \text{Dt}^2 \end{aligned} \quad (2)$$

4.3. Predicted Model Equation for Microhardness

The predicted model equation for microhardness from the analysis has been presented in Equation (3).

$$\ln(\text{HV}) = +4.24692 + 7.94843 \times 10^{-4} * \text{St} - 0.032930 * \text{Dwell time} + 5.6212 \times 10^{-5} * \text{St} * \text{Dt} \quad (3)$$

5. Model Adequacy Test

The model summary statistics for each response was recorded, the details of which have been discussed below:

5.1. Model Adequacy Test for Nitrogen Absorption

The model summary statistics for nitrogen absorption have been given in Table 10. It can be observed that the linear model for nitrogen absorption has been suggested by the design expert software.

Table 10. Model summary statistics for nitrogen absorption.

Source	Std. Dev.	R-Squared	Adjusted R-Squared	Predicted R-Squared	PRESS	
Linear	0.059	0.9778	0.9743	0.9665	0.069	suggested
2FI	0.061	0.9787	0.9733	0.9584	0.086	
Quadratic	0.051	0.9872	0.9802	0.9731	0.055	
Cubic	0.053	0.9919	0.9798	0.9323	0.14	
Quartic	0.057	0.9920	0.9761		+	Aliased

5.2. Model Adequacy Test for Density

The model summary statistics for density have been given in Table 11. It can be observed that the linear and cubic models for density has been suggested by the design expert software.

Table 11. Model summary statistics for density.

Source	Std. Dev.	R-Squared	Adjusted R-Squared	Predicted R-Squared	PRESS	
Linear	5×10^{-3}	0.8590	0.8373	0.7864	4×10^{-4}	suggested
2FI	4×10^{-3}	0.8741	0.8427	0.7751	5×10^{-4}	
Quadratic	4×10^{-3}	0.9221	0.8831	0.7315	6×10^{-4}	
Cubic	6×10^{-4}	0.9988	0.9969	0.5274	1×10^{-3}	suggested
Quartic	0.000	1.0000	1.0000		+	Aliased

5.3. Model Adequacy Test for Microhardness

The model summary statistics for micro hardness have been given in Table 12. It can be observed that the linear model for micro hardness has been suggested by the software.

Table 12. Model summary statistics for microhardness.

Source	Std. Dev.	R-Squared	Adjusted R-Squared	Predicted R-Squared	PRESS	
Linear	0.023	0.9462	0.9379	0.9182	0.010	suggested
2FI	0.023	0.9469	0.9337	0.9055	0.012	
Quadratic	0.025	0.9509	0.9264	0.8740	0.016	
Cubic	0.028	0.9633	0.9083	0.7729	0.028	
Quartic	0.030	0.9635	0.8906		+	Aliased

6. Optimization of the Responses

The optimization of the responses was obtained from the design expert software by considering the response value and desirability. The software suggested the optimum parameters combination. The details of the constraints and optimized responses are shown in Tables 13 and 14 respectively.

Table 13. Constraints of the process.

Constraints						
Name	Goal	Lower Limit	Upper Limit	Lower Weight	Upper Weight	Importance
A: St	is in range	1150	1200	1	1	3
B: Dt	is in range	1	8	1	1	3
N-abs	maximize	0.96	2.82	1	1	5
D	maximize	7.318	7.575	1	1	3
HV	maximize	180	235	1	1	4

Table 14. Suggested solutions for maximum output.

Number	St	Dt	N-abs	D	HV	Desirability	
1	1199.434	7.995	2.836	7.614	238.965	1.000	Selected
2	1199.751	7.956	2.823	7.615	238.740	1.000	
3	1200.000	8.000	2.850	7.617	239.178	1.000	
4	1199.226	7.981	2.825	7.612	238.795	1.000	
5	1199.946	7.956	2.827	7.616	238.797	1.000	
6	1199.631	7.999	2.842	7.615	239.057	1.000	
7	1198.868	7.999	2.827	7.611	238.836	1.000	
8	1199.537	7.966	2.823	7.614	238.757	1.000	
9	1198.588	7.999	2.821	7.609	238.752	1.000	
10	1199.819	7.986	2.839	7.616	239.012	1.000	
11	1197.444	8.000	2.799	7.603	238.418	0.995	

7. Experimental Validation Study

The validation of the developed models for the responses (N-abs, D and HV) was carried out by a confirmation test using the same procedure as discussed above. Thus, it becomes possible to authenticate the developed mathematical models. The optimum parameter settings not only improve the quality but also in the industries by reducing parts production time and cost. Therefore, the development of optimum parameters settings plays a major role in this context.

The experimental results of this study were in close agreement with the predicted values of the responses between them and was less than 2% as shown in Table 15.

Table 15. Experimental validation of the responses.

Response	Predicted	Experimental	% Error
N-abs	2.84977	2.82	1.05
D	7.61741	7.575	0.55
HV	239.178	235	1.77

8. Conclusions

This study analyzed and evaluated the results on the experimental application of modifying 316L stainless steel alloy surface with increased dwell time for simultaneous sintering and in situ surface nitriding. In this research, the feasibility of sintering process to simultaneously sinter and nitride the surface layer of 316L stainless steel alloy was tested and established successfully. The experimental results revealed that a significant amount of nitride layer was formed on the surface of the sintered samples. The XRD results revealed that the sintering parameters helped in diffusion of nitrogen into the matrix of 316L stainless steel. The diffusion resulted in the formation of nitrides of iron and carbon. The XPS results indicated the presence of nitrogen onto the surface of the sintered samples in the form of nitride layer. This nitride layer was also observed under optical microscope with a thickness of 6 μm . The nitrogen gas as sintering atmosphere, sintering temperature and increased dwell time for sintering of green compacts helped in increased properties of the samples. The nitrogen uptake increased the microhardness of the sintered samples by 27%. Nitrogen as the sintering atmosphere helped in nitrogen diffusion and surface nitriding of the sintered samples. Austenitic stainless steels have low hardness and wear resistance values, therefore, this nitride layer formation not only helps in improving surface layer but also increases the corrosion and wear resistance of the material. The best results in the form of densification, microhardness and nitrogen absorption were observed at 1200 °C and 8 h dwell time.

The influence of processing parameters on densification, microhardness, nitrogen absorption and spectroscopic properties were investigated. Further analysis to set the optimum parameters setting for

surface nitriding has been carried out. The mathematical model and equations for numerical prediction of densification, micro hardness and nitrogen absorption were also developed.

The newly modified approach of simultaneous sintering and surface nitriding was successful in addressing the related issues of this material.

The model and equations developed can be used to estimate the theoretical values of such responses by the industries for the production of implants and medical devices with desired properties. Moreover, the confirmation tests revealed that the experimental results are in close agreement with the predicted values of the responses with an error of less than 2%. This indicates that the developed model and equations are helpful in predicting material behavior in terms of its improved properties.

Author Contributions: Conceptualization, S.A.; formal analysis, S.A.; funding acquisition, A.M.A.R.; methodology, S.A.; project administration, A.M.A.R. and R.A.M.; resources, S.W.A. and A.A.A.A.; supervision, A.M.A.R. and R.A.M.; writing—original draft, S.A.; writing—review and editing, Z.B., S.H. and M.A.A.R. All authors have read and agreed to the published version of the manuscript.

Funding: This research was funded by YUTP-Fundamental Research grant and “The APC was funded by YUTP FRG, cost center, 015LC0-164”.

Acknowledgments: The authors would like to acknowledge Universiti Teknologi PETRONAS, Malaysia and National University of Sciences and Technology (NUST), Islamabad, Pakistan for carrying out research and other facilities.

Conflicts of Interest: The authors declare no conflict of interest.

References

1. Wiles, P. The classic: The surgery of the osteo-arthritis hip. *Clin. Orthop. Relat. Res.* **2003**, *417*, 3–16.
2. Wiles, P. The surgery of the osteo-arthritis hip. *Br. J. Surg.* **1958**, *45*, 488–497. [[CrossRef](#)] [[PubMed](#)]
3. Lo, K.H.; Shek, C.H.; Lai, J. Recent developments in stainless steels. *Mater. Sci. Eng. R Rep.* **2009**, *65*, 39–104. [[CrossRef](#)]
4. Ali, S.; Rani, A.; Altaf, K.; Baig, Z. Investigation of Boron addition and compaction pressure on the compactibility, densification and microhardness of 316L Stainless Steel. *IOP Conf. Ser. Mater. Sci. Eng.* **2018**, *344*, 012023. [[CrossRef](#)]
5. Disegi, J.; Eschbach, L. Stainless steel in bone surgery. *Injury* **2000**, *31*, D2–D6. [[CrossRef](#)]
6. Dewidar, M. Influence of processing parameters and sintering atmosphere on the mechanical properties and microstructure of porous 316L stainless steel for possible hard-tissue applications. *Int. J. Mech. Mech. Eng.* **2012**, *12*, 10–24.
7. Talha, M.; Behera, C.; Sinha, O. A review on nickel-free nitrogen containing austenitic stainless steels for biomedical applications. *Mater. Sci. Eng. C* **2013**, *33*, 3563–3575. [[CrossRef](#)]
8. Alvarez, K.; Sato, K.; Hyun, S.; Nakajima, H. Fabrication and properties of Lotus-type porous nickel-free stainless steel for biomedical applications. *Mater. Sci. Eng. C* **2008**, *28*, 44–50. [[CrossRef](#)]
9. Niinomi, M.; Nakai, M.; Hieda, J. Development of new metallic alloys for biomedical applications. *Acta Biomater.* **2012**, *8*, 3888–3903. [[CrossRef](#)]
10. Muley, S.V.; Vidvans, A.N.; Chaudhari, G.P.; Udainiya, S. An assessment of ultra fine grained 316L stainless steel for implant applications. *Acta Biomater.* **2016**, *30*, 408–419. [[CrossRef](#)]
11. Wong, J.Y.; Bronzino, J.D.; Peterson, D.R. *Biomaterials: Principles and Practices*; CRC Press: Boca Raton, FL, USA, 2012.
12. Bronzino, J.D.; Peterson, D.R. *Biomedical Engineering Fundamentals*; CRC press: Boca Raton, FL, USA, 2014.
13. Bronzino, J.D. *Biomedical Engineering Handbook*; CRC press: Boca Raton, FL, USA, 1999; Volume 2.
14. Park, J.B. *Biomaterials Science and Engineering*; Springer Science & Business Media: Berlin, Germany, 2012.
15. Saini, M.; Singh, Y.; Arora, P.; Arora, V.; Jain, K. Implant biomaterials: A comprehensive review. *World J. Clin. Cases WJCC* **2015**, *3*, 52. [[CrossRef](#)] [[PubMed](#)]
16. Yang, K.; Ren, Y. Nickel-free austenitic stainless steels for medical applications. *Sci. Technol. Adv. Mater.* **2010**, *11*, 014105. [[CrossRef](#)] [[PubMed](#)]

17. Cordeiro, J.M.; Beline, T.; Ribeiro, A.L.R.; Rangel, E.C.; da Cruz, N.C.; Landers, R.; Faverani, L.P.; Vaz, L.G.; Fais, L.M.; Vicente, F.B.; et al. Development of binary and ternary titanium alloys for dental implants. *Dent. Mater.* **2017**, *33*, 1244–1257. [[CrossRef](#)] [[PubMed](#)]
18. Mirza, A.; King, A.; Troakes, C.; Exley, C. Aluminium in brain tissue in familial Alzheimer’s disease. *J. Trace Elem. Med. Biol.* **2017**, *40*, 30–36. [[CrossRef](#)] [[PubMed](#)]
19. Vahter, M.; Berglund, M.; Åkesson, A.; Liden, C. Metals and women’s health. *Environ. Res.* **2002**, *88*, 145–155. [[CrossRef](#)]
20. Bhola, R.; Bhola, S.M.; Mishra, B.; Olson, D.L. Corrosion in titanium dental implants/prostheses—A review. *Trends Biomater. Artif. Organs* **2011**, *25*, 34–46.
21. Manam, N.; Harun, W.; Shri, D.; Ghani, S.; Kurniawan, T.; Ismail, M.; Ibrahim, M.H. Study of corrosion in biocompatible metals for implants: A review. *J. Alloys Compd.* **2017**, *701*, 698–715. [[CrossRef](#)]
22. Chen, Q.; Thouas, G.A. Metallic implant biomaterials. *Mater. Sci. Eng. R Rep.* **2015**, *87*, 1–57. [[CrossRef](#)]
23. Singh, R.; Dahotre, N.B. Corrosion degradation and prevention by surface modification of biometallic materials. *J. Mater. Sci. Mater. Med.* **2007**, *18*, 725–751. [[CrossRef](#)]
24. Liu, X.; Chu, P.K.; Ding, C. Surface modification of titanium, titanium alloys, and related materials for biomedical applications. *Mater. Sci. Eng. R Rep.* **2004**, *47*, 49–121. [[CrossRef](#)]
25. Dayss, E.; Leps, G.; Meinhardt, J. Surface modification for improved adhesion of a polymer–metal compound. *Surf. Coat. Technol.* **1999**, *116*, 986–990. [[CrossRef](#)]
26. Huang, Y.; Qu, Y.; Yang, B.; Li, W.; Zhang, B.; Zhang, X. In vivo biological responses of plasma sprayed hydroxyapatite coatings with an electric polarized treatment in alkaline solution. *Mater. Sci. Eng. C* **2009**, *29*, 2411–2416. [[CrossRef](#)]
27. Ali, S.; Rani, A.; Majdi, A.; Mufti, R.A.; Hastuty, S.; Hussain, M.; Shehzad, N.; Baig, Z.; Aliyu, A.; Azeez, A. An Efficient Approach for Nitrogen Diffusion and Surface Nitriding of Boron-Titanium Modified Stainless Steel Alloy for Biomedical Applications. *Metals* **2019**, *9*, 755. [[CrossRef](#)]
28. Ali, S.; Rani, A.; Majdi, A.; Mufti, R.A.; Azam, F.I.; Hastuty, S.; Baig, Z.; Hussain, M.; Shehzad, N. The Influence of Nitrogen Absorption on Microstructure, Properties and Cytotoxicity Assessment of 316L Stainless Steel Alloy Reinforced with Boron and Niobium. *Processes* **2019**, *7*, 506. [[CrossRef](#)]
29. Ali, S.; Rani, A.M.; Altaf, K.; Hussain, P.; Prakash, C.; Hastuty, S.; Rao, T.V.; Subramaniam, K. Investigation of Alloy Composition and Sintering Parameters on the Corrosion Resistance and Microhardness of 316L Stainless Steel Alloy. In *Advances in Manufacturing II*; Springer: Cham, Switzerland, 2019; pp. 532–541.



© 2020 by the authors. Licensee MDPI, Basel, Switzerland. This article is an open access article distributed under the terms and conditions of the Creative Commons Attribution (CC BY) license (<http://creativecommons.org/licenses/by/4.0/>).